# Crystal Structures of Adrenodoxin Reductase in Complex with $NADP^+$ and NADPH Suggesting a Mechanism for the Electron Transfer of an Enzyme Family[†,‡]

Gabriele A. Ziegler and Georg E. Schulz*

*Institut für Organische Chemie und Biochemie, Albert-Ludwigs-Universität, Albertstrasse 21, D-79104 Freiburg im Breisgau, Germany*

*Received January 13, 2000; Revised Manuscript Received June 19, 2000*

ABSTRACT: Adrenodoxin reductase is a flavoenzyme that shuffles electrons for the biosynthesis of steroids. Its chain topology belongs to the glutathione reductase family of disulfide oxidoreductases, all of which bind FAD at equivalent positions. The three reported structures of adrenodoxin reductase were ligated with reduced and oxidized NADP and have now confirmed this equivalence also for the NADP-binding site. Remarkably, the conformations and relative positions of the prosthetic group FAD and the cofactor NADP have been conserved during protein evolution despite very substantial changes in the polypeptide. The ligated enzymes showed small changes in the domain positions. When compared with the structure of the NADP-free enzyme, these positions correspond to several states of the domain motion during NADP binding. On the basis of the observed structures, we suggest an enzymatic mechanism for the subdivision of the received two-electron package into the two single electrons transferred to the carrier protein adrenodoxin. The data banks contain 10 sequences that are closely related to bovine adrenodoxin reductase. Most of them code for gene products with unknown functions. Within this family, the crucial residues of adrenodoxin reductase are strictly conserved. Moreover, the putative docking site of the carrier is rather well conserved. Five of the family members were assigned names related to ferredoxin:$NADP^+$ reductase, presumably because adrenodoxin reductase was considered a member of this functionally similar family. Since this is not the case, the data bank entries should be corrected.

Adrenodoxin reductase (AdR,[1] EC 1.18.1.2) is an FAD-containing enzyme that catalyzes the electron transfer from NADPH to the electron carrier adrenodoxin. This reaction represents the first step in the mitochondrial cytochrome P450 electron-transfer systems (*1*−*4*). The mitochondrial cytochromes P450 are involved in a variety of reactions including the conversion of cholesterol into pregnenolone, which is the first and rate-limiting step in the biosynthesis of all steroids. Since steroids are widely used as drugs and since they constitute major antiinflammatory, anti-cancer, and contraceptive agents, they are a subject of intensive research. Recently, the first two steps of the steroidogenic pathway were reproduced in *Saccharomyces cerevisiae* so that pregnenolone could be derived from the simple carbon source galactose (*5*). This biosynthesis was engineered by co-expression of six genes including those of the bovine proteins AdR, adrenodoxin, and cytochrome P450scc.

Enzymes resembling mitochondrial cytochromes P450 have not yet been detected in lower eukaryotes. However, a gene from *S. cerevisiae* with a sequence identity of approximately 35% to mammalian AdR was cloned, and the gene product Arh1p was shown to substitute the mammalian enzyme in the electron-transfer chain. Arh1p is essential for yeast viability (*6*); its biological role remains unknown. A further adrenodoxin-like system exists in insects because mitochondrial cytochrome P450 from the house fly, which is involved in the metabolism of xenobiotics, was shown to be reduced by bovine mitochondrial AdR and adrenodoxin (*7*). These observations together with the sequence similarity between AdR and a number of yet uncharacterized genes from pro- and eucaryotes in the data banks suggest that adrenodoxin-like electron transport systems are ubiquitous.

The crystal structure of bovine AdR had been solved by X-ray diffraction at 1.7 Å resolution (*8*). AdR consists of two domains with similar chain topologies, one for binding the prosthetic group FAD while the other had been suggested to bind the cofactor NADP (Figure 1). The NADP domain is inserted after the fourth central $\beta$-strand of the FAD domain, which is a characteristic feature of the disulfide oxidoreductases (*9*). The similarity with the disulfide oxidoreductases is remarkable as AdR does not transfer two-electron packages but belongs to the large group of electron transferases that subdivide the two-electron packages from NAD(P) into single electrons (*10*). Except for AdR, all structurally established enzymes of this group share the plant ferredoxin:$NADP^+$ reductase (FNR) fold (*11*−*16*). Here we report the crystal structures of three complexes between AdR and NADPH or $NADP^+$, confirming the predicted cofactor binding site and suggesting an electron transfer mechanism

[†] The project was supported by the Deutsche Forschungsgemeinschaft under SFB-388.

[‡] The coordinates and structure factors are deposited with the Protein Data Bank as files 1E1K, 1E1L, 1E1M, and 1E1N.

* To whom correspondence should be addressed. Phone: +49-761-203-6058. Fax: +49-761-203-6161. E-mail: schulz@bio.chemie.uni-freiburg.de.

[1] Abbreviations: AdR, bovine adrenodoxin reductase; FNR, plant ferredoxin: $NADP^+$ reductase; GR, glutathione reductase; rmsd, root-mean-square deviation.

10.1021/bi000079k CCC: $19.00 
Published on Web 08/17/2000

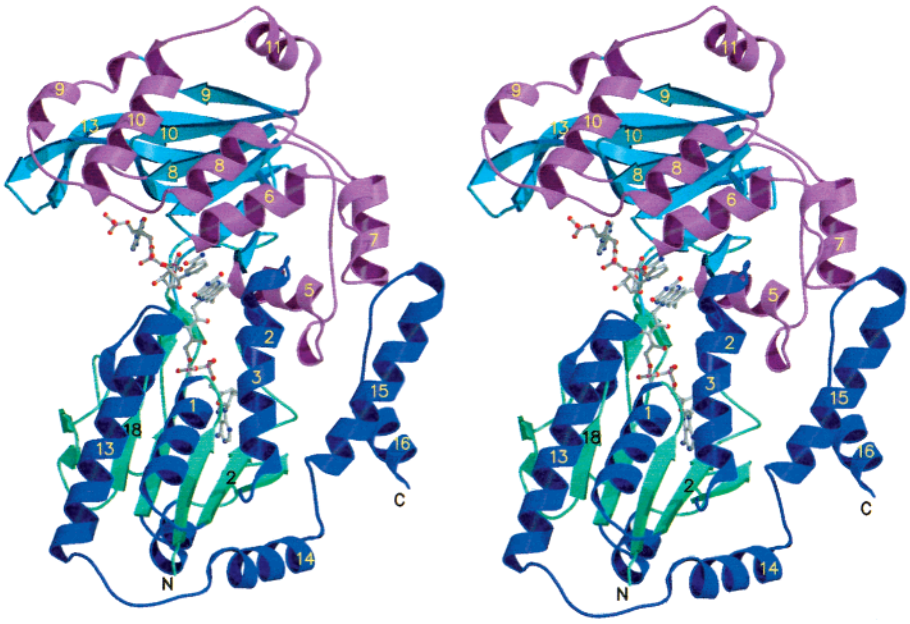


FIGURE 1: Complex AdR:NADP$^+$(cocryst) illustrating the AdR chain topology. NADP$^+$ and FAD are depicted as ball-and-stick models. The colors differentiate between domains. Some α-helices and $\beta$-strands are labeled. In all AdR structures residues 1 to 5 are invisible indicating that they are mobile.

based on the observed changes. In addition, we have analyzed the sequence-related genes with respect to their likely functions.

## MATERIALS AND METHODS

*Crystal Production.* The recombinant bovine adrenodoxin reductase was expressed in *Escherichia coli* strain BL21(DE3) which contained a plasmid encoding the HSP60-chaperone system (*17*). After induction, the temperature was lowered to 20 °C. AdR was isolated by ion exchange- and affinity chromatography. All crystals were grown with the hanging drop vapor diffusion method at 20 °C. The droplet contained buffer C (50 mM sodium cacodylate, pH 6.5, 100 mM calcium acetate) with 4 mg/mL protein, 5% glycerol and 8% (w/v) PEG-8000, whereas the reservoir consisted of 12% (w/v) PEG-8000 in buffer C (*17*). The complex AdR:NADP$^+$(cocryst) was obtained by cocrystallization with 0.5 mM NADP$^+$. All crystals were stepwise transferred into cryo-protectant buffer containing 20% glycerol and 12% PEG-8000 in buffer C. Subsequently, they were mounted on a loop, shock-frozen in a 100 K nitrogen gas stream and kept at this temperature.

Since cocrystallization attempts with NADPH failed, crystals were soaked for 45 min with 4 mM NADPH in cryo-protectant buffer to obtain the complex AdR:NADPH; longer soaks destroyed the crystals. The yellow color of the crystals vanished, indicating that the enzyme was being reduced. The direct soak in the cryo-protectant buffer was necessary, because these crystals were extremely unstable. Moreover, it minimized the risk of reoxidation. A further complex, AdR:NADP$^+$(soak) was obtained by the same procedure except that the additive was 4 mM NADP$^+$. Again the crystals cracked during longer soaks.

*Data Collection, Structure Analyses, and Comparisons.* All X-ray diffraction measurements were performed at 100 K. Synchrotron radiation at beamline BW7B of the EMBL-outstation Hamburg was used for complexes AdR:NADP$^+$(cocryst) and AdR:NADPH, and a rotating anode (Rigaku RU200B) for complex AdR:NADP$^+$(soak). In all cases, the X-ray detectors were image plates (MARresearch). The data were processed with the programs MOSFLM (*18*) and SCALA (*19*). Structure factors were calculated using the program TRUNCATE (*19*).

The high-resolution structure of NADP-free AdR in crystal form A′ (*8*) was used to analyze the structures of the complexes. The AdR model was transferred into the unit cell of the respective complex crystal and refined using the program REFMAC (*19*) in combination with the bulk solvent correction of X-PLOR (*20*). The resulting model was used to phase ($F_o - F_c$)- and ($2F_o - F_c$)-maps that revealed the bound NADP molecules and other differences. Ordered water molecules were automatically generated with program ARP (*19*).

After establishing its structure, AdR was related to other enzymes with similar chain folds or sequences. All data for glutathione reductase (GR) were from the *E. coli* enzyme, the coordinates of which are deposited as file 1GET in the Protein Data Bank (*21*). The sequence alignment was performed with program CLUSTALW (*22*). The solvent-accessible surface was calculated using a probe radius of 1.4 Å in program NACCESS (*23*). The figures were produced using programs MOLSCRIPT (*24*) and ALSCRIPT (*25*).

## RESULTS AND DISCUSSION

*Structure Analyses.* AdR uses NADPH as the reducing cofactor. The NADP-binding site has already been predicted from the chain fold similarity between AdR and the disulfide oxidoreductases (*8*). Now we report the actual binding site and the conformational changes during the binding process as observed with one cocrystallized and two soaked crystalline complexes (Tables 1 and 2). All analyses were based on the known structure of NADP-free AdR in crystal form A′ at 1.7 Å resolution (*8*). The obtained data quality is

Table 1: X-ray Diffraction Data

| AdR complexes | $NADP^+$(cocryst) | $NADP^+$(soak) | NADPH |
|---|---|---|---|
| space group[a] | $P2_1$ | $P2_1$ | $P2_1$ |
| cell dimensions | | | |
| *a* (Å) | 59.5 | 60.9 | 61.5 |
| *b* (Å) | 62.8 | 62.4 | 62.5 |
| *c* (Å) | 85.3 | 78.2 | 78.6 |
| $\beta$ (deg) | 108.2 | 106.6 | 106.7 |
| wavelength (Å) | 0.847 | 1.54 | 0.847 |
| resolution (Å) | 30−2.25 | 26−1.95 | 28−1.85 |
| unique reflections | 28 171 | 41 157 | 47 193 |
| redundancy[b] | 3.4 (3.4) | 3.6 (3.6) | 3.2 (2.9) |
| completeness (%)[b] | 99 (99) | 100 (100) | 96 (91) |
| $R_{sym}$ (%)[b,c] | 5.9 (31) | 6.9 (33) | 4.4 (15) |
| $I/\sigma_I$[b] | 8.7 (2.4) | 9.9 (2.3) | 12.3 (5.0) |
| $R_{iso}$ (%) | | 20.6 | 17.6 |

[a] All data were collected at 100 K. NADP-free AdR is always crystal form A′ in space group $P2_1$ with $a = 60.8$ Å, $b = 62.5$ Å, $c = 78.4$ Å, and $\beta = 106.8°$ (*8*). A second crystal form A″ of NADP-free AdR in to space group $P2_1$ with $a = 57.8$ Å, $b = 62.0$ Å, $c = 83.0$ Å and $\beta = 107.1°$ had been used for the initial phasing (*8*). Its crystal packing corresponds to AdR:$NADP^+$(cocryst). [b] The last shell values are given in parentheses. [c] $R_{sym} = \sum_{hkl,i}| I_{hkl,i} - \langle I_{hkl}\rangle|/\sum_{hkl,i} I_{hkl,i}$.

Table 2: Structural Refinement Statistics

| AdR complexes | $NADP^+$ (cocryst) | $NADP^+$ (soak) | NADPH |
|---|---|---|---|
| resolution range (Å) | 15−2.3 | 29−1.95 | 18−1.85 |
| number of polypeptide atoms | 3504 | 3504 | 3504 |
| number of NADP and FAD atoms | 101 | 101 | 101 |
| number of solvent molecules | 110 | 350 | 395 |
| $R_{cryst}$ (%) | 21.9 | 18.4 | 18.8 |
| $R_{free}$ (%) (5% random test set) | 27.9 | 22.7 | 22.8 |
| rmsd bond lengths (Å) | 0.016 | 0.012 | 0.015 |
| rmsd bond angles (deg) | 2.9 | 2.4 | 2.4 |
| average *B*-factor (Å$^2$) | 59 | 27 | 23 |

demonstrated by a difference-omit map of bound $NADP^+$ for the reported structure with the lowest resolution in Figure 2. In the following we consider complex AdR:$NADP^+$(cocryst) to show the structure of bound NADP, and we regard the two soaked complexes as intermediates of the NADP-binding process.

The main structural difference between AdR:$NADP^+$-(cocryst) and NADP-free AdR is in a displacement of the NADP domain (residues 109−329) relative to the FAD domain (residues 1−108, 330−460) as derived from a superposition of the "cores" of the FAD domains (Figure 3). This constitutes a small induced fit with a maximum deviation of 2.5 Å at residue 232 on helix α9. The superimposed 66 residues of the two FAD domain cores showed an rmsd of 0.3 Å and therefore no significant differences.

The observed domain movement is accompanied by a slight change in the molecular packing scheme giving rise to a distinct crystal form of the cocrystals with a *c*-axis prolonged by 7 Å (Table 1). Moreover, one of the two main crystal packing contacts is diminished in the cocrystals (Table 3). This explains why this complex could not be obtained by soaking. The lack of sufficient packing interactions affects the *B*-factors, which are particularly high in the cocrystallized complex (Table 2), but fortunately did not prevent us from detecting all residues as well as $NADP^+$ and FAD in the electron density maps.

*NADP-Binding Mode.* As predicted (*8*), NADP-binding closely resembles that of the disulfide oxidoreductases (Figure 4). The polar binding contacts are listed in Table 4. $NADP^+$ docks in an extended conformation with the adenine and nicotinamide rings in the usual *anti*-conformation like NADPH in GR and related proteins (*26*). Most of the $NADP^+$ contacts are with residues of the NADP domain (Figure 1). As in GR, the adenine moiety of $NADP^+$ is stacked between an isoleucine (Ile329) and an arginine (Arg197) and forms no hydrogen bond to the protein. The 2′-phosphate is fixed

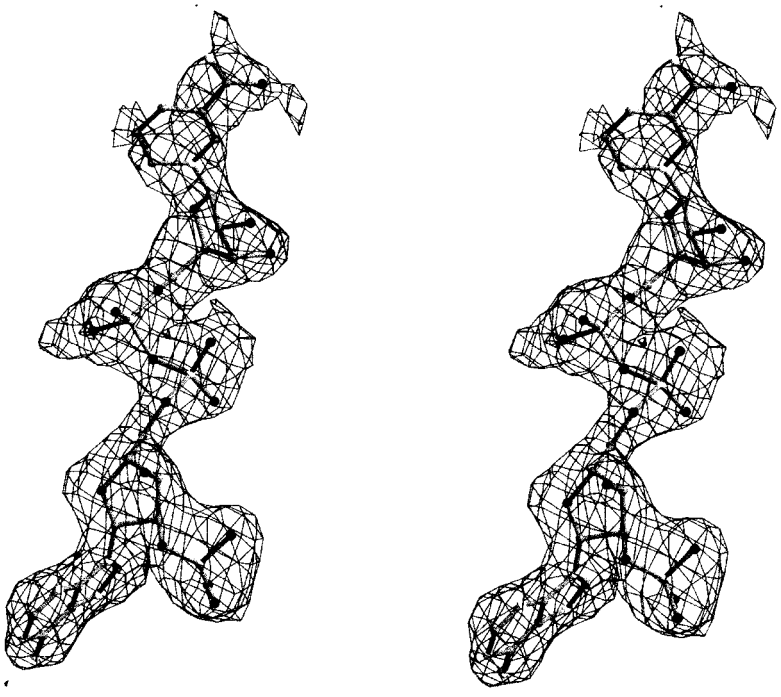

FIGURE 2: $NADP^+$ as bound in complex AdR:$NADP^+$(cocryst) together with the $(F_o - F_c)$-difference-omit map for the $NADP^+$ molecule at 2.3 Å resolution. The map is contoured at 2.0$\sigma$. The N- and O-atoms are indicated by white and black balls, respectively.

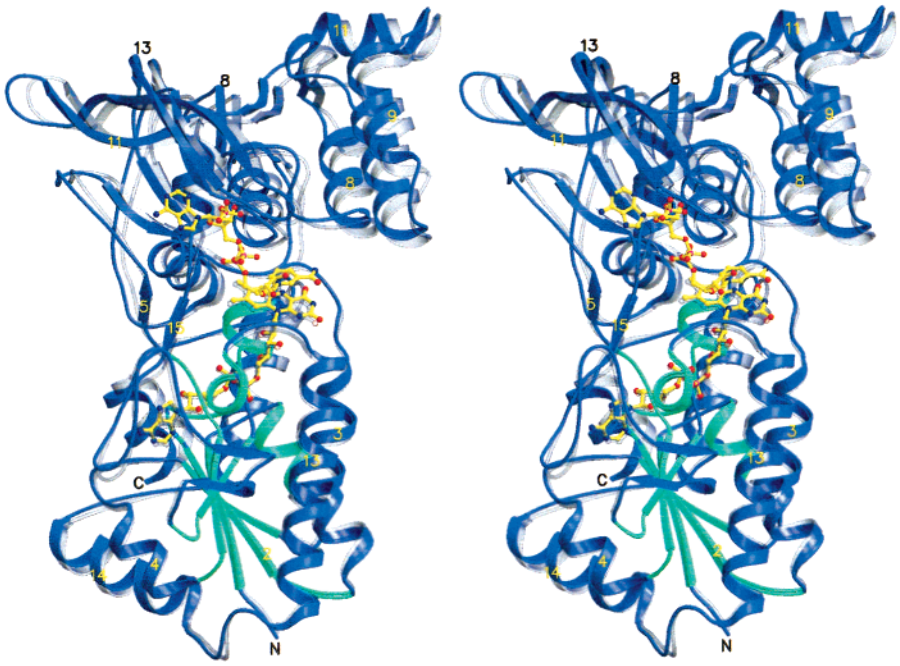


FIGURE 3: Stereoview of the induced fit upon NADP-binding. NADP-free AdR in crystal form A′ is transparent and complex AdR:NADP$^+$(cocryst) is blue. FAD and NADP$^+$ are given as ball-and-stick models. The superposition is based on the "core" of the FAD domain (green) which consists of residues 8−22, 30−51, 74−78, 94−105, and 359−370. Some α-helices and $\beta$-strands are labeled.

Table 3: Crystal Contacts in NADP-free AdR and in Complex AdR:NADP$^+$(cocryst)[a]

| contact[b] | contact area[c] (Å$^2$) | contact residue ensembles[d] | no. of hydrogen bonds |
|---|---|---|---|
| I−II | 674 (232) | a−b (c−d) | 7 (1) |
| I−III | 572 (628) | e−f (g−h) | 10 (5) |
| I−IV | 290 (271) | i−j (k−l) | 7 (3) |
| I−V | 87 (47) | m−n (m−o) | 5 (1) |
| I−VI | − (44) | − (p−q) | − (1) |

[a] All data are for NADP-free AdR in crystal form A′ (*8*); the data for AdR:NADP$^+$(cocryst) are in parentheses. The contacts of the second crystal form A″ of NADP-free AdR (*8*) are essentially identical to those of AdR:NADP$^+$(cocryst), except that contact I−VI does not exist in form A″. [b] Contacts between the reference molecule I at (x,y,z) and the 5 symmetry-related molecules II($-x+1$, $y-0.5$, $-z$), III($-x$, $y-0.5$, $-z$), IV($-x+1$, $y-0.5$ , $-z+1$), V($x$, $y-1$, $z$), and VI($x+0.5$, $y$, $z$). [c] Buried solvent-accessible surface of the reference molecule. The total buried surface of the reference molecule on crystallization is 3246 Å$^2$ (or 16%) and 2444 Å$^2$ (or 12%) for NADP-free AdR and complex AdR:NADP$^+$(cocryst), respectively. [d] Contacting residues are defined as burying more than 1 Å$^2$ solvent-accessible surface on crystallization. The residue ensembles are $a$ = 212, 215, 244, 267; $b$ = 70, 72, 428−429, 436; $c$ = 57; $d$ = 429; $e$ = 240, 353, 355, 388, 392−393; $f$ = 93, 396, 405, 412, 416−417; $g$ = 240, 388, 392; $h$ = 93, 395, 416−417; $i$ = 301, 303−304, 310; $j$ = 288−290; $k$ = 301, 304; $l$ = 288−289; $m$ = 240; $n$ = 415−416, 418; $o$ = 416; $p$ = 439; $q$ = 398.

by the guanidinium groups of Arg197 and Arg198; the remaining part of NADP$^+$ contacts the protein predominantly via main chain atoms (Table 4). Both riboses exhibit the *2′*-endo conformation, which is common in disulfide oxidoreductases that use NAD and more seldom in those using NADP (*26*−*29*).

The binding of the oxidized nicotinamide moiety of NADP$^+$ at oxidized FAD is an interesting feature of AdR because such a binding has never been observed in the disulfide oxidoreductases, where the oxidized nicotinamide either pointed away like in trypanothione reductase (*27*) and lipoamide dehydrogenase (*28*) or was disordered like in GR (*26*). Only the reduced nicotinamide moiety was bound in a sandwich-like structure at the isoalloxazine of such enzymes placing its C4 atom adjacent to the N5 atom of FAD (*26*, *29*, *30*). In AdR the C4 atom of the oxidized nicotinamide is at the N5 atom of FAD, as to be expected in a hydride transfer. In contrast to the disulfide oxidoreductases, however, the nicotinamide ring is not parallel to the isoalloxazine rings but forms an angle of about 20°. The nicotinamide position is stabilized by a strong hydrogen bond (2.4 Å) between its carboxamide and the carboxyl group of the strictly conserved Glu209. A similar tilted interaction has been reported for a designed mutant of FNR (*31*), where the angle was 30° as compared to the 20° observed in AdR. In this mutant a tyrosine side chain that covered the N5 atom of FAD in NADP-free FNR had been replaced by a serine, which obviously opened the binding site for the crystal study.

These observations agree with experiments using solvated electrons to reduce AdR in the presence of NADP$^+$, which resulted in nicotinamide reduction followed by electron transfer to the isoalloxazine (*32*). Similar experiments with electron transferases of the FNR-type in the presence of NADP$^+$ caused a direct reduction of the isoalloxazine, indicating that it was not shielded by a bound nicotinamide. Obviously, the FNR-type enzymes do not bind NADP$^+$ easily.

*Putative Induced Fit Intermediates.* In addition to AdR:NADP$^+$(cocryst), we produced a further NADP$^+$ complex by soaking a crystal of form A′ with NADP$^+$. In this complex, named AdR:NADP$^+$(soak), the nicotinamide ring had almost the same lateral distance to the isoalloxazine as in AdR:NADP$^+$(cocryst), but its conformation was less favorable for electron transfer because it entered the binding site only halfway (Figure 5). With respect to the AdR:NADP$^+$(cocryst) structure the nicotinamide ring remained 1 Å nearer to the solvent. We therefore suggest that this soaked structure represents an intermediate of the induced fit movements during NADP-binding.

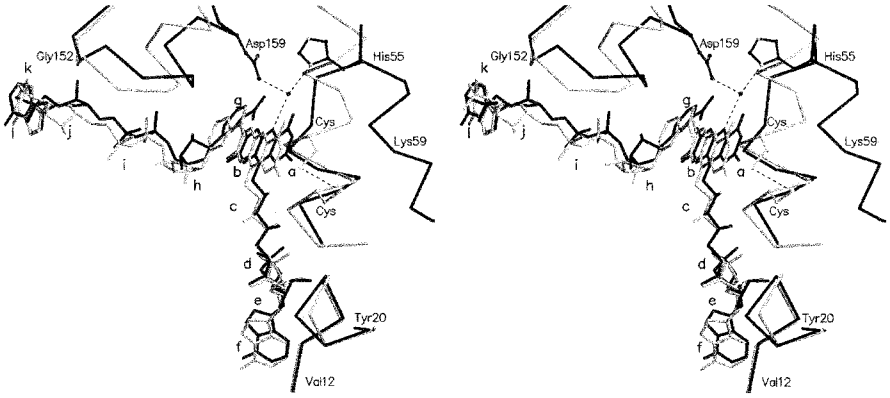


FIGURE 4: Superposition of complex AdR:NADP$^+$(cocryst)(dark lines) with that of reduced glutathione reductase and NADPH (light lines) (*21*, *29*) as based on the FAD domain cores (Figure 3). Residues His55 and Asp159 of AdR and the redoxactive disulfide of GR are shown as ball-and-stick models, all others are given as $C^\alpha$ plots. Some further residues of AdR are labeled. After averaging over the five AdR structures, the relative *B*-factors of FAD parts *a* to *f* are 122, 105, 99, 86, 93, and 96%, respectively. In a given structure, the relative *B*-factors are defined as the average *B*-factor of the atoms within a particular part divided by the average *B*-factor of all FAD atoms. In complex AdR:NADP$^+$(cocryst) the relative *B*-factors of NADP$^+$ parts *g* to *l* are 112, 98, 91, 95, 96, and 109%, respectively. The corresponding values of AdR:NADP$^+$(soak) are 146, 128, 100, 83, 83, and 61%, respectively, resembling those of AdR:NADPH.

Table 4: Polar Interactions between AdR and NADP

| | | distances (Å) | | |
|---|---|---|---|---|
| NADP atom[a] | protein atom | AdR:NADP$^+$ (cocryst) | AdR:NADP$^+$ (soak) | AdR:NADPH |
| C4N | FAD-N5 | 3.1 | 3.2 | 3.4 |
| N7N | Glu209-OE2 | 2.4 | 2.3 | 2.4 |
| O2*[b] | Asn155-ND2 | 3.4 | 3.4 | |
| O3*[b] | Gly374-N | 2.9 | | |
| | Thr373-O | | 2.4 | 2.5 |
| O1N[c] | Asn155-N | | 3.6 | |
| | Val156-N | 3.2 | 3.3 | 3.6 |
| O2N[c] | Gly330-N | | | 3.6 |
| | Tyr331-O | | | 3.4 |
| O3′[d] | Gln153-N | 2.8 | 3.3 | |
| O4′[d] | Ser328-O | | 3.6 | |
| O1B[e] | Arg197-NH2 | | | 3.4 |
| | Arg198-NH1 | 3.5 | 3.0 | 3.5 |
| O2B[e] | Arg197-NH1 | 3.4 | 2.7 | |
| | Arg198-NE | 2.9 | 2.5 | 2.4 |
| | Arg198-NH1 | | 3.3 | 3.0 |
| O3B[e] | Arg197-NE | | | 2.7 |
| | Arg197-NH1/2 | 2.7 | | 3.1 |

[a] Nomenclature as issued by program REFMAC (*19*). [b] Oxygen atoms of the nicotinamide ribose, which is in *2′*-endo conformation. [c] Phosphate oxygen of the nicotinamide moiety. [d] Oxygen atoms of the adenine ribose, which is in *2′*-endo conformation. [e] Oxygen atoms of the 2′-phosphate.

In a further experiment we soaked a crystal of form A′ with the reduced cofactor NADPH to obtain complex AdR:NADPH. The resulting binding mode of NADPH was virtually identical to that of NADP$^+$ in AdR:NADP$^+$(soak) (Figure 5). In both cases the soaking times were limited to 45 min because longer exposures cracked the crystals. We therefore conclude that both soaks were terminated before the cofactor could enter its binding site completely and cause the NADP domain displacement and packing rearrangement (Table 3) that destroys the crystal.

To outline the induced fit motions, we superimposed the three complex structures with their FAD domain cores (marked in Figure 3) on NADP-free AdR (crystal form A′) and evaluated the motion of the NADP domain (Figure 5). We refrained from interpreting this motion as a rotation because the rotation axes of the three complexes differed strongly from each other, rendering the rotation angles incompatible. Instead, we calculated the shift vectors of the centers of NADP domain masses relative to those of the NADP-free AdR. The resulting shift vectors were approximately collinear with lengths of 0.4, 0.5, and 1.5 Å for the complexes AdR:NADPH, AdR:NADP$^+$(soak), and AdR:NADP$^+$(cocryst), respectively. Accordingly, the two soaked complexes can be considered as structural intermediates of the induced fit motion of the domain.

A reexamination of crystal form A″ of NADP-free AdR, the quality of which was inferior to crystal form A′ because its resolution reached merely 2.4 Å (*8*), revealed essentially the same packing scheme as the cocrystals with NADP$^+$ (Table 3) and also a prolonged *c*-axis (legend of Table 1). Crystal form A″ was rare; it grew at the same condition as the common crystal form A′. Superimposing the FAD domain cores of the AdR molecule in crystal form A″ with that in form A′ revealed an NADP domain displacement that was intermediate between those of AdR:NADP$^+$(soak) and AdR:NADP$^+$(cocryst). The corresponding shift vector had a length of 0.7 Å and was approximately collinear to the others (see above). We therefore conclude that the form A″ packing contacts froze an AdR conformation halfway between the NADP-free AdR of crystal form A′ and AdR:NADP$^+$(cocryst). Since form A″ had essentially the same packing scheme as the cocrystals (Table 3), we suggest that the NADP domain is intrinsically mobile in the NADP-free enzyme such that the small crystal packing forces suffice to freeze it at any position.

*Mobility Differences.* The *B*-factor averages and distributions of the two soaked complexes closely resembled those of NADP-free AdR in crystal form A′ before soaking. In contrast, the average *B*-factor of the cocrystallized complex was much higher (Table 2). This *B*-factor increase concerned the whole polypeptide together with FAD and the bound cofactor NADP$^+$; it was particularly pronounced in the NADP domain. Since this increase was rather uniform, we suggest that it does not report a higher peptide mobility but that diminished packing contacts (Table 3) gave rise to some crystal disorder. This view is supported by a similar *B*-factor increase in crystal form A″ as compared to form A′ (*8*), because form A″ has the same packing scheme as the cocrystals.

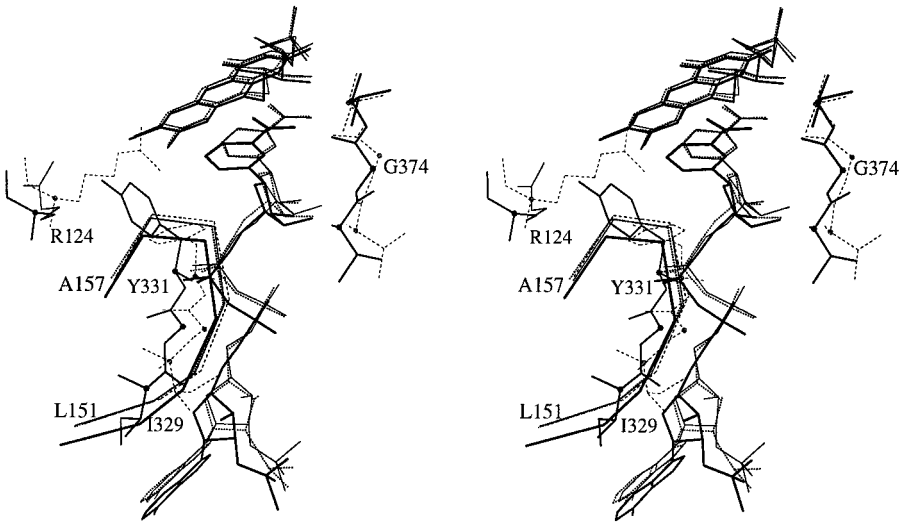


FIGURE 5: Induced fit motions on NADP-binding outlined by the superposition of NADP-free AdR (crystal form A′, dashed line) with complexes AdR:NADPH (thin line), AdR:$NADP^+$(soak) (dotted line) and AdR:$NADP^+$(cocryst) (thick line). All superpositions are based on the FAD domain cores (Figure 3). Peptide segment 151−157 is part of the sequence fingerprint for dinucleotide-binding (*35*) and depicted as $C^\alpha$ plot for all structures. For clarity, the other peptide segments, namely Arg124, Ile329−Tyr331, and Thr373−Val375, are only shown for NADP-free AdR and AdR:$NADP^+$(cocryst). The AMP-moiety of FAD is omitted. $C^\alpha$ atoms are marked by dots. Peptide bond 373−374 flips over, Tyr331, and Arg124 move away.

The *B*-factor distributions along the FAD molecules resembled each other in all five examined AdR structures. The most rigid part of FAD was the pyrophosphate, and most flexible was the isoalloxazine (Figure 4). Moreover, the pteridine moiety of the isoalloxazine was significantly more mobile than the benzene, which corresponded to the proposed role of the latter in the electron transfer (*8*). Interestingly, also in GR (*21*, *29*) the pteridine mobility is higher than that of benzene, although its N3 atom forms a tight hydrogen bond to a backbone carbonyl group.

The *B*-factor distributions along the NADP molecules in complexes AdR:NADPH and AdR:$NADP^+$(soak) showed a gradient from a rigidly bound adenine to a more mobile nicotinamide with a stepwise increase at the pyrophosphate (Figure 4). A similar *B*-factor gradient was observed for NADPH as bound to GR in a soaking experiment (*21*, *29*). After cocrystallization, however, $NADP^+$ bound more uniformly to the polypeptide, resulting in a rather flat *B*-factor distribution in AdR:$NADP^+$(cocryst). This difference in conjunction with the observed incomplete positioning of nicotinamide in the soaked complexes indicates that the adenosine moiety of NADP binds first to the enzyme and the nicotinamide moiety binds thereafter.

*Electron-Transfer Mechanism.* Apart from the domain movements upon NADP binding, the three AdR complexes show some interesting details. For example, peptide 373−374 flips during the docking process (Figure 5). At the initial stages, it uses its carbonyl to bind the O3* atom of the nicotinamide ribose; after flipping over on complete NADP-binding in AdR:$NADP^+$(cocryst), it binds O3* with its amide (Table 4). Position 374 contains a strictly conserved glycine (see below Figure 8). Moreover, the strictly conserved Tyr331 moves upon NADP docking and pushes Arg124 away. Tyr331 is a close neighbor-along-the-chain of Ile329 that accommodates the adenine of NADP together with the strictly conserved Arg197. In all three NADP complexes there is a strong hydrogen bond between the amide of the nicotinamide moiety and the strictly conserved Glu209 as depicted in Figure 6. Furthermore, all of them contain a water molecule fixed between the strictly conserved His55 and Asp159 near the N5 atom of the isoalloxazine. The position of this water molecule changes slightly (Figure 6). Taken together these data suggest the electron-transfer scheme of Figure 7.

The proposed mechanism has been based on the structures of NADP-free AdR (*8*) and of AdR:$NADP^+$(cocryst). The two soaked complexes AdR:NADPH and AdR:$NADP^+$(soak) are merely taken as intermediates of the docking process. We suggest that in the NADP-free structure (upper left side in Figure 7) His55 is neutral and Asp159 as well as Glu209 are charged and that there is no hydrogen bond between the water and the N5 atom of FAD. The protonation states of these three residues correspond to the pH of 7.9 within mitochondria (*33*). The missing hydrogen bond between N5 and the water agrees with the observed N to O distance of 3.5 Å (Figure 6). The hydroxyl of Tyr331 is at a distance of 8.6 Å to the N5 atom and thus much further away from the flavin than the tyrosine occupying the nicotinamide binding site of FNR (*31*).

As a first step NADPH binds to AdR, displacing Tyr331 and Arg124 together with quite a number of water molecules that are not shown in Figure 7. The resulting structure is derived from AdR:$NADP^+$(cocryst). A hydride ion is transferred from the C4 atom of NADPH to the N5 atom of FAD which causes a charge separation to $NADP^+$ and $FADH^-$. The transferred hydrogen forms a perfect hydrogen bond to the water with a length of 3.1 Å (Figure 6). $FADH^-$ agrees with the observation that soaking in NADPH removes the yellow color of the crystals as observed in AdR:NADPH.

In a second step the electron carrier adrenodoxin docks at AdR and receives the first electron, giving rise to an $NADP^+$ complex with AdR containing the neutral semiquinone $FADH^\bullet$, which is sketched at the lower right side of Figure 7. The blue semiquinone has been observed (*32*). Moreover, adrenodoxin docking in the presence of $NADP^+$ agrees with experimental data (*34*) and with our docking model (*8*). Since

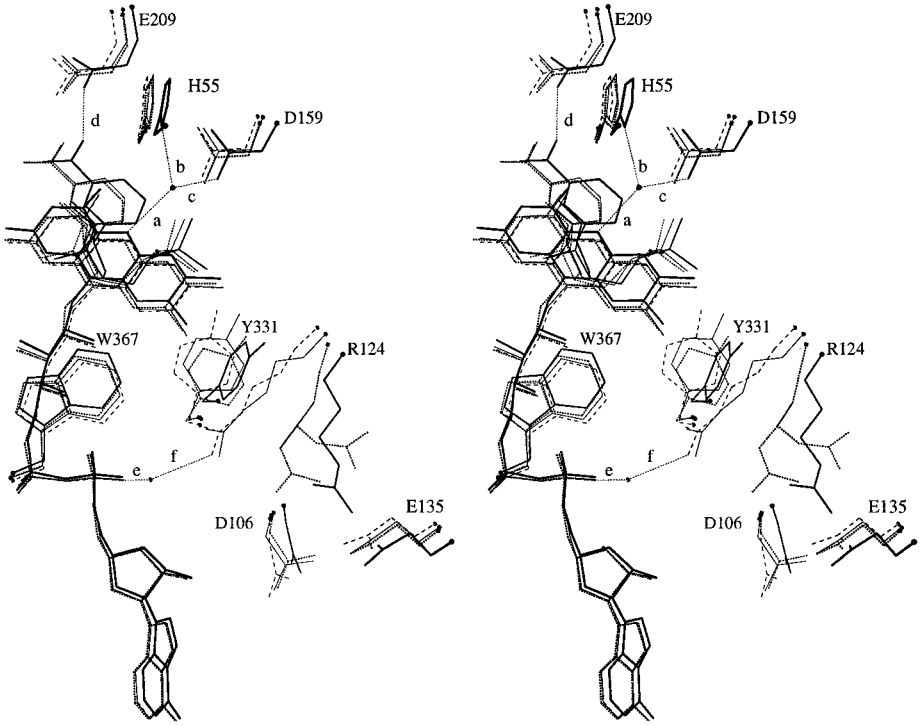


FIGURE 6: Induced fit processes around FAD showing NADP-free AdR (dashed line) with complexes AdR:NADPH (thin line), AdR:NADP$^+$(soak) (dotted line, Arg124 in two conformations), and AdR:NADP$^+$(cocryst) (thick line). The superposition is based on the FAD domain cores. The lengths of the hydrogen bonds *a* to *f* in the order NADP-free AdR (form A′), AdR:NADPH, AdR:NADP$^+$(soak), and AdR:NADP$^+$(cocryst) are *a* (3.5, 3.4, 3.2, 3.1 Å), *b* (2.9, 2.9, 2.9, 3.2 Å), *c* (2.6, 2.7, 2.7, 2.8 Å), *d* (none, 2.4, 2.3, 2.4 Å), *e* (2.7, 2.6, 2.6, 2.8 Å), and *f* (2.9, 3.7 Å, none, none), respectively. Chain cuts are marked by dots.

this model had been derived for NADP-free AdR, we reexamined it for AdR:NADP$^+$(cocryst) and found that it was neither affected by the bound NADP$^+$ nor by the small NADP domain displacement.

As the third step, we suggest that NADP$^+$ dissociates, leaving AdR with FADH$^\bullet$ hydrogen bonded with its N5 atom to the central water molecule (lower left of Figure 7). The NADP-binding pocket is refilled with water (not shown in Figure 7) as observed in the NADP-free AdR structure (*8*). This water is in close contact to the depicted fixed central water between His55 and Asp159. Moreover, Tyr331 and Arg124 are reinstalled at their original positions. The guanidinium group of Arg124 is at van der Waals distance to the C7α methyl group of FAD and to the strictly conserved Trp367, which has been suggested to participate in the electron transfer from the isoalloxazine to the carrier (*8*). At this position, the positively charged Arg124 facilitates the electron transfer between FAD and Trp367.

The fourth step then involves the transfer of the second electron to a second docked adrenodoxin molecule. We propose that the second transfer requires the facilitation by Arg124 because the driving force for this process is smaller than that for the first electron. Concomitantly with the electron transfer, the N5 proton moves over to the central water where it is buffered by His55 and then released to the contacting other water molecules (filling the NADP-binding site) and eventually to the bulk solvent. The proposed mechanism is consistent with the observed data. It constitutes a working hypothesis waiting for future experiments.

*Sequence Comparison.* A search through databases PIRONLY, TREMBL, and SWISSPROT revealed 10 sequences with amino acid identities above 35% when compared to AdR and no other relationships above the

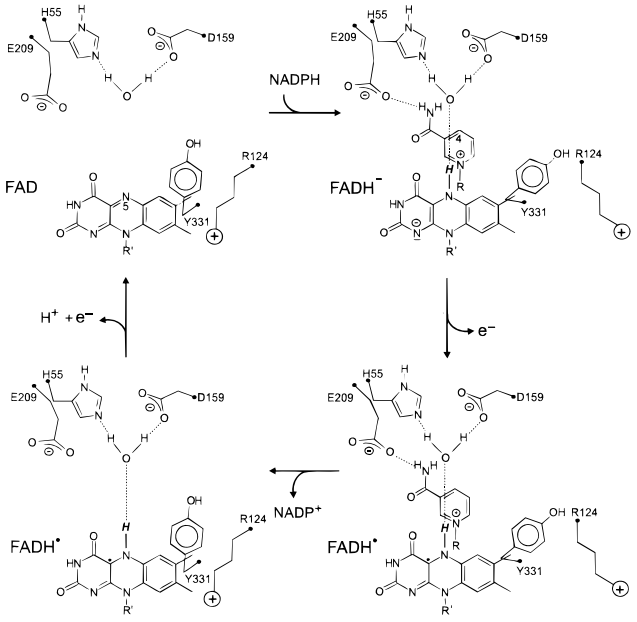


FIGURE 7: Proposed electron-transfer mechanism in AdR in view of the two structures of NADP-free AdR (*8*) and AdR:NADP$^+$-(cocryst). The two soaked structures are merely considered as likely intermediates of the NADPH docking process. NADP-free AdR (upper left) receives NADPH, which transfers a hydride ion to produce NADP$^+$ and FADH$^-$ (upper right). The docking process displaces Tyr331 and Arg124. FADH$^-$ transfers one electron to a docking adrenodoxin molecule forming the neutral blue semiquinone (lower right). NADP$^+$ is released and Tyr331 together with Arg124 return to their starting positions (lower left). FADH$^\bullet$ transfers the second electron to a second adrenodoxin molecule and its N5 proton moves over to the depicted central water molecule, which in turn releases it to the contacting bulk water.

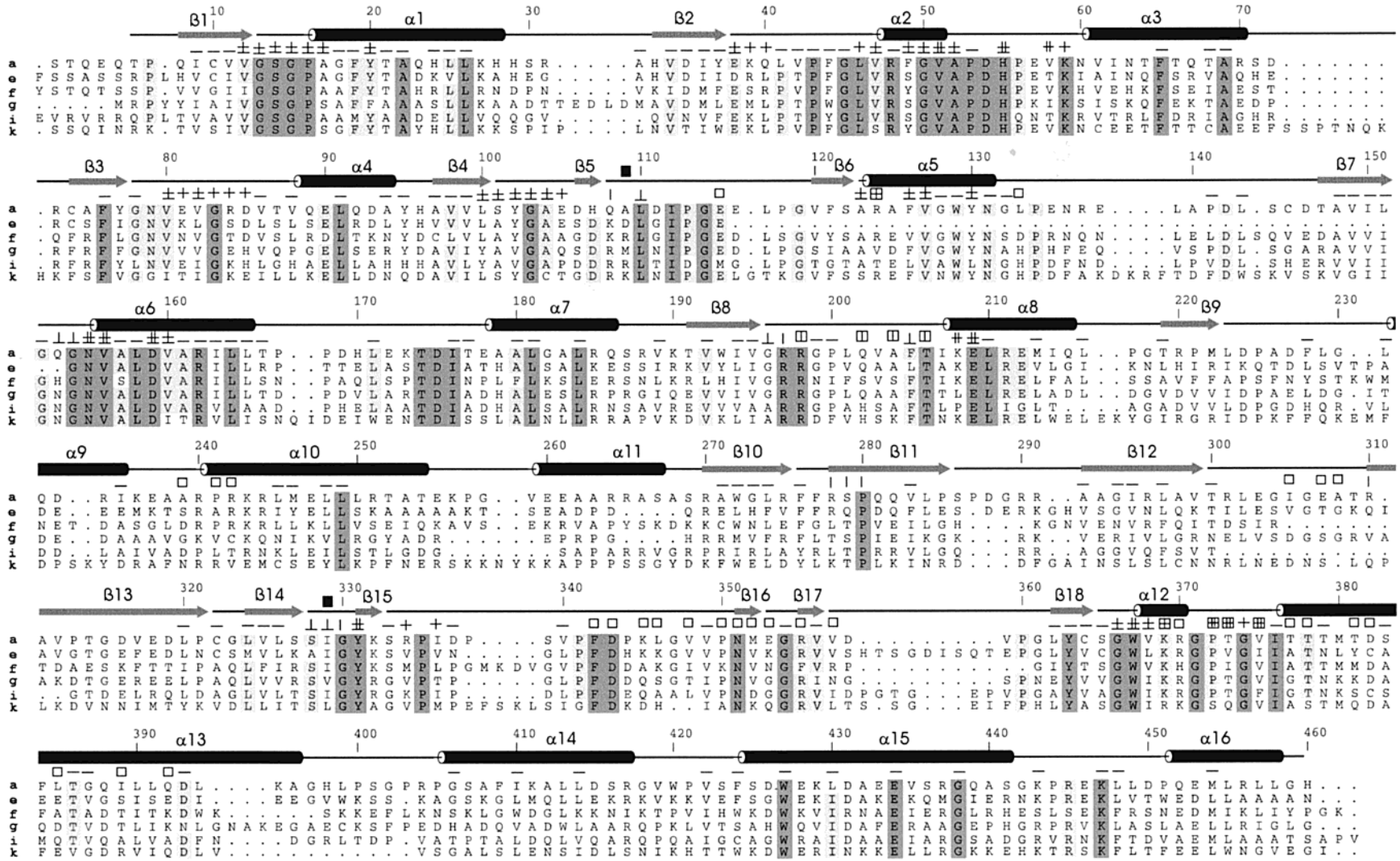

FIGURE 8: Sequence alignment of bovine AdR (*37*) with related proteins as calculated in a search with HUSAR (*38*) using CLUSTALW with a gap penalty of 8.0 and a gap separation penalty range of 0.8 (*22*). The sequences *a* to *k* are identified in the legend of Table 5, their average sequence identity is 37%. Identical residues are darkened. The numbers, the secondary structure elements, and the positional marks are for sequence *a* of bovine AdR in the top line. The domain borders are at the black squares. The DNA-derived sequence *e* seems to err between positions 116 and 153 (see text). The positional marks denote residues with an atom within 6 Å distance from FAD (+) and $NADP^+$ (|) as well as residues that are covered (more than 20 $Å^2$) by a docking adrenodoxin molecule (□) according to an earlier model (*8*). Internal residues with less than 10% of their surface being solvent-accessible are marked by (−). The marks are overlaid for residues falling in more than one of the groups. The assignments were derived from the structure AdR:$NADP^+$(cocryst).

Table 5: Sequence Comparison Matrix Stating Percentages of Identical Residues

| accession[a,b] | | b | c | d | e | f | g | h | i | j | k |
|---|---|---|---|---|---|---|---|---|---|---|---|
| sw:P08165 | a | 87 | 87 | 88 | 46 | 40 | 42 | 41 | 39 | 37 | 36 |
| sw:P56522 | b | | 95 | 87 | 46 | 41 | 43 | 40 | 39 | 37 | 35 |
| sw:Q61578 | c | | | 87 | 47 | 41 | 43 | 41 | 39 | 37 | 35 |
| sw:P22570 | d | | | | 47 | 42 | 43 | 41 | 40 | 38 | 36 |
| tr:O49356 | e | | | | | 37 | 39 | 38 | 38 | 39 | 31 |
| tr:O59710 | f | | | | | | 37 | 35 | 32 | 32 | 34 |
| pr:A70905 | g | | | | | | | 82 | 43 | 43 | 32 |
| tr:O32886 | h | | | | | | | | 42 | 41 | 35 |
| sw:Q10547 | i | | | | | | | | | 77 | 30 |
| tr:O33064 | j | | | | | | | | | | 30 |

[a] a, AdR (bovine); b, AdR (rat); c, AdR (mouse); d, AdR (human); e, "Ferredoxin:$NADP^+$ reductase-like protein" (*Arabidopsis thaliana*); f, "Ferredoxin:$NADP^+$ reductase" (*Schizosaccharomyces pombe*); g, "Rv0174" (*Mycobacterium tuberculosis*); h, "Possible ferredoxin" (*Mycobacterium leprae*); i, "Putative ferredoxin:$NADP^+$ reductase" (*Mycobacterium tuberculosis*); j, "Ferredoxin" (*Mycobacterium leprae*); k, Arh1p from *Saccharomyces cerevisiae* with accession code sw:P48360 was isolated and shown to substitute for AdR (*6*). The names from *e* through *j* are taken from the data banks. All names referring to "ferredoxin" are wrong (see text). [b] The databases are sw, SWISSPROT; tr, TREMBL; pr, PIRONLY.

background. The sequence comparison matrix is given in Table 5. This degree of homology points to similar structures and functions. An alignment of the six sequences with less than 50% mutual residue identities is shown in Figure 8. The conservation is most striking in the active center of AdR as can be recognized from the marked residues around FAD and NADP, which also contain the common GxGxxG(A) sequence fingerprints of dinucleotide binding (*35*). It is therefore likely that all of these enzymes have the same chain fold relation to the glutathione reductase family of disulfide oxidoreductases as AdR. Since residues 46−55 and 171−179 at the interface between the FAD- and NADP domains are highly conserved (Figure 8), however, none of the AdR family members should resemble the disulfide oxidoreductase thioredoxin reductase with its highly mobile NADP domain (*36*).

Highly indicative for the same electron transfer function as AdR are the strictly conserved residues His55 and Asp159 that hold the crucial water molecule at the N5 atom of FAD (Figure 6). Characteristic for AdR are also the strictly conserved residues Glu209, Tyr331 (working as a lever to displace Arg124), and Trp367, which most likely accepts the electrons from the benzene moiety of FAD for transfer to adrenodoxin (*8*). The conserved residues Arg197 and Arg198 confirm that all of these gene products use NADP and not NAD. Moreover, quite a number of internal residues are conserved demonstrating the close structural similarity within this family (Figure 8). For analyzing the conservation of the adrenodoxin docking site, we took our model (*8*) and selected the 27 residues that lost more than 20 $Å^2$ of their solvent-accessible surface on docking. These residues are marked in Figure 8, they comprise at least two well-conserved sequence segments, indicating that also the carrier docking site is conserved within the family.

It should be noted that sequence *e* from the *Arabidopsis* genome lacks residues 116−153. This gap includes the first two residues of the dinucleotide-binding sequence fingerprint (*35*). Moreover, the borders at positions 115 and 154 cannot be connected to each other if they were following the AdR structure, which however, is highly probable because the border regions themselves are strongly conserved. This contradiction points either to a sequencing error or to a *pseudo*-gene.

Unfortunately, five of the family members were assigned names related to the FNR family (Table 5), presumably because AdR was thought to belong to this family. The sequence alignment of Figure 8, however, demonstrates that all of them are structurally and functionally closely similar to AdR. Since AdR differs from FNR with respect to chain fold and reaction geometry [NADPH docks at the (*Re*) side of the isoalloxazine of AdR as compared to the (*Si*) side in FNR], we conclude that AdR and FNR resemble each other only functionally. As a consequence, the eleven sequences of Table 5 represent a separate and new enzyme family, which contains AdR as a the best characterized member. We therefore suggest to call it "AdR family".

## ACKNOWLEDGMENT

We thank the EMBL team at DESY (Hamburg) for helping with synchrotron data collection and T. Schwede and C. Vonrhein for discussions.

## REFERENCES

1. Omura, T., Sanders, E., Estabrook, R. W., Cooper, D. Y., and Rosenthal, O. (1966) *Arch. Biochem. Biophys. 117*, 660−673.
2. Lambeth, J. D., Seybert, D. W., Lancaster, J. R., Jr., Salerno, J. C., and Kamin, H. (1982) *Mol. Cell. Biochem. 45*, 13−31.
3. Hanukoglu, I. (1992) *J. Steroid Biochem. Mol. Biol. 43*, 779−804.
4. Bernhardt, R. (1996) *Rev. Physiol., Biochem. Pharmacol. 127*, 137−221.
5. Duport, C., Spagnoli, R., Degryse, E., and Pompon, D. (1998) *Nat. Biotechnol. 16*, 186−189.
6. Lacour, T., Achstetter, T., and Dumas, B. (1998) *J. Biol. Chem. 273*, 23984−23992.
7. Guzov, V. M., Unnithan, G. C., Chernogolov, A. A., and Feyereisen, R. (1998) *Arch. Biochem. Biophys. 359*, 231−240.
8. Ziegler, G. A., Vonrhein, C., Hanukoglu, I., and Schulz, G. E. (1999) *J. Mol. Biol. 289*, 981−990.
9. Schulz, G. E. (1980) *J. Mol. Biol. 138*, 335−347.
10. Massey, V. (1995) *FASEB J. 9*, 473−475.
11. Karplus, P. A., Daniels, M. J., and Herriott, J. R. (1991) *Science 251*, 60−66.
12. Correll, C. C., Batie, C. J., Ballou, D. P., and Ludwig, M. L. (1992) *Science 258*, 1604−1610.
13. Lu, G., Campbell, W. H., Schneider, G., and Lindqvist, Y. (1994) *Structure 2*, 809−821.
14. Nishida, H., Inaka, K., Yamanaka, M., Kaida, S., Kobayashi, K., and Miki, K. (1995) *Biochemistry 34*, 2763−2767.
15. Wang, M., Roberts, D. L., Paschke, R., Shea, T. M., Masters, B. S. S., and Kim, J.-J. P. (1997) *Proc. Natl. Acad. Sci. U.S.A. 94*, 8411−8416.
16. Ingelman, M., Bianchi, V., and Eklund, H. (1997) *J. Mol. Biol. 268*, 147−157.
17. Vonrhein, C., Schmidt, U., Ziegler, G. A., Schweiger, S., Hanukoglu, I., and Schulz, G. E. (1999) *FEBS Lett. 443*, 167−169.
18. Leslie, A. G. W. (1990) In *Crystallographic Computing 5* (Moras, D., Podgarny, A. D., and Thierry, J. C., Eds.) pp 50−61, Oxford University Press, Oxford, U.K.
19. CCP4, Collaborative Computational Project Number 4. (1994) *Acta Crystallogr., Sect. D 50*, 760−763.
20. Brünger, A. T. (1993) *X-PLOR version 3.1 a system for X-ray crystallography and NMR*, Yale University Press, New Haven.
21. Mittl, P. R. E., and Schulz, G. E. (1994) *Protein Sci. 3*, 799−809.

22. Thompson, J. D., Higgins, D. G., and Gibson, T. J. (1994) *Nucleic Acids Res. 22*, 4673−4680.
23. Hubbard, S. J., and Thornton, J. M. (1993) *NACCESS*, Computer Program, Department of biochemistry and molecular biology, University College, London.
24. Kraulis, P. J. (1991) *J. Appl. Crystallogr. 24*, 946−950.
25. Barton, G. J. (1993) *Protein Eng. 6*, 37−40.
26. Karplus, P. A., and Schulz, G. E. (1989) *J. Mol. Biol. 210*, 163−180.
27. Bailey, S., Smith, K., Fairlamb, A. H., and Hunter, W. N. (1993) *Eur. J. Biochem. 213*, 67−75.
28. Mattevi, A., Obmolova, G., Sokatch, J. R., Betzel, C., and Hol, W. G. (1992) *Proteins: Struct., Funct., Genet. 13*, 336−351.
29. Mittl, P. R. E., Berry, A., Scrutton, N. S., Perham, R. N., and Schulz, G. E. (1994) *Protein Sci. 3*, 1504−1514.
30. Lantwin, C. B., Schlichting, I., Kabsch, W., Pai, E. F., and Krauth-Siegel, R. L. (1994) *Proteins: Struct., Funct., Genet. 18*, 161−173.
31. Deng, Z., Aliverti, A., Zanetti, G., Arakaki, A. K., Ottado, J., Orellano, E. G., Calcaterra, N. B., Ceccarelli, E. A., Carillo, N., and Karplus, P. A. (1999) *Nat. Struct. Biol. 6*, 847−853.
32. Kobayashi, K., Miura, S., Miki, M., Ichikawa, Y., and Tagawa, S. (1995) *Biochemistry 34*, 12932−12936.
33. Llopis, J., McCaffery, J. M., Miyawaki, A., Farquhar, M. G., and Tsien, R. Y. (1998) *Proc. Natl. Acad. Sci. U.S.A. 96*, 6803−6808.
34. Miura, S., and Ichikawa, Y. (1994) *J. Biol. Chem. 269*, 8001−8006.
35. Schulz, G. E. (1992) *Curr. Opin. Struct. Biol. 2*, 61−67.
36. Waksmann, G., Krishnan, T. S. R., Williams, C. H., Jr., and Kuriyan, J. (1994) *J. Mol. Biol. 236*, 800−816.
37. Sagara, Y., Takata, Y., Miyata, T., Hara, T., and Horiuchi, T. (1987) *J. Biochem. 102*, 1333−1336.
38. Senger, M., Glatting, K. H., Ritter, O., and Suhai, S. (1995) *Comput. Methods Prog. Biomed. 46*, 131−141.

BI000079K